IEEE Access
Multidisciplinary | Rapid Review | Open Access Journal

Received October 10, 2021, accepted November 10, 2021, date of publication November 12, 2021,
date of current version November 22, 2021.

Digital Object Identifier 10.1109/ACCESS.2021.3127947

Design and Multi-Objective Optimization of a Dexterous Mobile Parallel Mechanism for Fusion Reactor Vacuum Vessel Assembly

CHANGYANG LI[1], HUAPENG WU[1], AND HARRI ESKELINEN[2]
[1]Laboratory of Intelligent Machine, LUT University, 53850 Lappeenranta, Finland
[2]Laboratory of Production Engineering, LUT University, 53850 Lappeenranta, Finland

Corresponding author: Changyang Li (changyang.li@lut.fi)

This work has been carried out within the framework of the EUROfusion Consortium and has received funding from the Euratom research and training program 2014-2018 and 2019-2020 under grant agreement No 633053. The views and opinions expressed herein do not necessarily reflect those of the European Commission.

ABSTRACT The present paper presents a newly designed dexterous mobile parallel mechanism for fusion reactor vacuum vessel assembly, the robot system has advantages in terms of compact design, the capability to carry out heavy-duty machining tasks, evacuation, and has less space occupation compared to other robot systems in existence. Despite different robot systems are studied in the fusion reactor, there is still a lack of research on mechanism development for vacuum vessel assembly, which is attractive to future fusion reactors. In the fusion reactor, the robot systems will carry out different tasks, such as welding and machining. The assembly tasks of the vacuum vessel will be performed from inside of the vacuum vessel on-site. Then the paper introduces the single-objective and multi-objective optimization design of the proposed mechanism, the optimized objective is considered to be a combination of parallel mechanism dynamic machining force, dexterity, stiffness, and workspace volume. The design variables are derived from the geometry of the fixed and movable platforms, which include mass, inertia, the sizes of the platforms, and distances between universal joints located on the platforms. In the multi-objective optimization, non-dominated sorting genetic algorithm II is adopted and different trajectories are designed to simulate the machining process, which further turns the local optimization problem into a global optimization problem. Finally, the optimized results are extracted and analyzed. Simulation results indicate the effectiveness of the proposed multi-objective optimization approaches and multi-objective optimization is found to be more reliable than single-objective optimization.

INDEX TERMS Mobile robots, parallel robots, optimization, fusion reactors.

I. INTRODUCTION

A. FUSION REACTOR

Fusion is the energy source of the sun and the stars; the most efficient fusion reactor is identified as the reaction between two hydrogen isotopes, deuterium, and tritium. Unlike fission reactors, nuclear fusion can provide virtually safe, affordable and limitless clean energy for the world. The machine where this reactor happens is called tokamak. Fusion energy generated from a thermonuclear fusion reactor is one of the greatest challenges of this century. International organizations and many countries are developing and building test fusion reactors, such as the International Thermonuclear Experimental Reactor (ITER), the Europe Demonstration power plant (EU DEMO), the Chinese Fusion Engineering Testing Reactor (CFETR), Japan Torus-60SA (JT-60SA) and Korean DEMO (K-DEMO) [1]–[5].

The largest of the global fusion projects ITER, involves collaboration of 35 nations. ITER tokamak mainly consists of magnets, a vacuum vessel, a blanket, a divertor and a cryostat, among which the fusion reactor vacuum vessel (VV) shown in Figure.1 is a torus shape with a 6.2 m plasma major radius, a double-wall structure, weights 8000 tonnes, whose primary function is to provide a high-quality vacuum for the plasma. According to literature [6], the VV sector should have less than ± 10 mm tolerances of the overall profile in ITER and ± 8 mm in CFETR [7]. Hence, the VV must be manufactured and assembled at a high-quality level; the accuracy of

The associate editor coordinating the review of this manuscript and approving it for publication was Guilin Yang.

the welding position is required to be ±0.5 mm [2]. In the assembly process of VV in ITER, a stainless steel 316L splice plate of 40-60 mm thickness has to be prepared, transported and welded first to one sector of VV; a slow deposition rate with several passes generates relatively high heat to the plate, which causes undesired deformation. The extra Non-Destructive Testing (NDT) and machining process must be carried out to compensate for the deformation caused by the heat, and, to avoid further assembly error, finally tailor the surface quality to meet the required level, and the splice plate can be welded to another VV sector [8].

In VV assembly and maintenance, lots of assembly work must be carried out by an on-site robotic machine. On-site assembly ensure the accurate alignment, especially of the large components in VV and the magnet system, and also takes the economic impact of transporting large components from the workshop to the site. In addition, the assembly work of VV must be carried out from inside to ensure the accuracy of the assembly [9].

In ITER, this positional tolerances for the largest components, such as VV and magnetic coils, are as low as 2 mm. The assembly and maintenance usually cannot be performed by a commercial computer numerical control (CNC) machine or general industrial robot, or other heavy machine working from outside the VV, because they cannot achieve high mobility, capability of working in small space, high accuracy and high structure stiffness at the same time. Literature [10] proposed the 10-DoF intersector welding robot (IWR) shown in Figure.1 to carry out the heavy-duty machining and welding processes inside the VV. The IWR can move to any position on a double track rail mounted on the VV inner wall, including 360° vertical and lateral rotation. The concept design of portable machines introduced in literature [9], [11] borrowed the double-track rail idea from literature [10], but they could only achieve mid-duty milling and drilling operations.

In JT-60SA, considering the transportation convenience, the inboard and outboard segments are first fabricated at a factory first, then the VV segments are transported on-site and joined together by different welding technology (an assembly process of a 40° VV sector is shown in Figure.2). Firstly, direct butt welding is performed along welding paths 1, 2 and 3, then splice plate welding is performed along other welding paths. The design of VV sectors must take welding shrinkage into consideration, as well as the splice plates to ensure that the whole VV is assembled as designed, which is important for further fusion reactions. To achieve consistent and high-accuracy welding, the automatic manipulator was applied to the direct butt welding process [5], [12].

However, the structure of the IWR and portable machines still have many drawbacks, such as heavy weight, difficult to evacuate if breakout happens, and the double-track rail occupies too much space, for other relatively small fusion reactor such as CFETR and JT60-SA, the port is too small to allow the pass of the robot systems. Therefore, previous double-track rail concept has to be optimized to single-track rail concept, and then the mobile parallel mechanism also needs to be developed into a lighter version so that the system has enough stiffness and mobility to carry out different tasks. Several technical problems and requirements are listed below to point out the greatest difficulties of designing the robot system in fusion reactor:

1) The assembly work has to be carried out inside VV on-site;
2) The robot system should have mobility and heavy-duty work capability;
3) The robot system should be compact and easy to transfer.

B. PARALLEL MECHANISM OPTIMIZATION

Nowadays, parallel and series robots are widely used in industry. Parallel manipulator has relatively high stiffness and payload capacity than series robots [13]–[15]. There are also different configurations of parallel manipulator, 2-,3-,4-, and 5-Degree of Freedom (DOF) parallel manipulator designs are systematically introduced in literature [16], which illustrates details of the joints, links, kinematics and degree of freedoms of different parallel manipulator configurations on a theoretical level. Applications that adapt a parallel manipulator can also be found in many fields [17], such as high-speed lifting robots in food packaging and precision surgery, former application increases the accuracy and efficiency in food packaging factory and free labors from repeat work. The latter can eliminate the potential surgery failure possibly caused by human errors. Since the parallel robots are used in different fields, the purpose of the parallel robots differs, which can be easily concluded from previously mentioned applications, given that one requires high speed, and the other one requires high accuracy. These arouse the research on optimization of the parallel robot.

One important component of the optimization is that there is no perfect optimization of every aspect, optimization on one or several objectives is practical and reasonable. There were many objective functions that came up for each researcher. One of the most classic objective proposed in related literature [18] was called dexterity, which was derived from the Jacobian matrix. Another famous objective proposed in literature related [19] was called manipulability. Stiffness is another important property of the parallel robot, which expresses the ability of the robot to resist deformation in response to external forces; the stiffness was studied in literature on the topics [20]–[24] and it was used as one objective function in different forms to optimize the robot's performance. The objectives mentioned above were derived mainly from the kinematic models, where external dynamic disturbance, mass properties, forces, or inertia of the mass were neglected. When the dynamic of the robot is taken into consideration, the model becomes more complicated than the kinematic model; for example, machining force should be considered in a heavy-duty work environment, there were research derives different objective functions from the dynamic model, such as dynamic dexterity

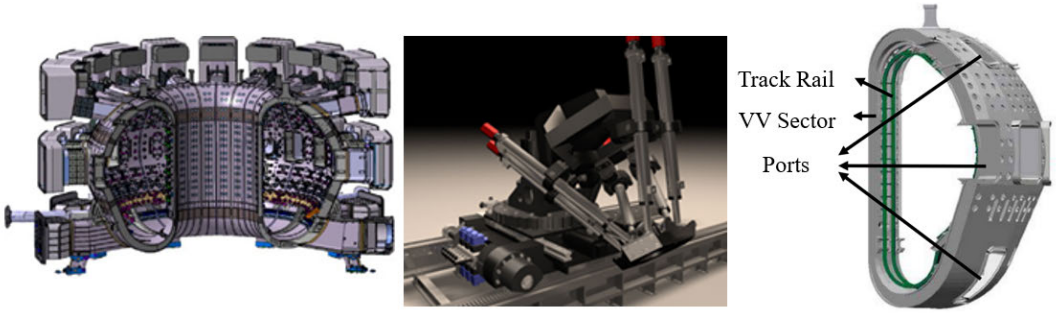

FIGURE 1. ITER section view (left), 3D model of IWR for ITER (middle), VV sector, track rail and ports (right).

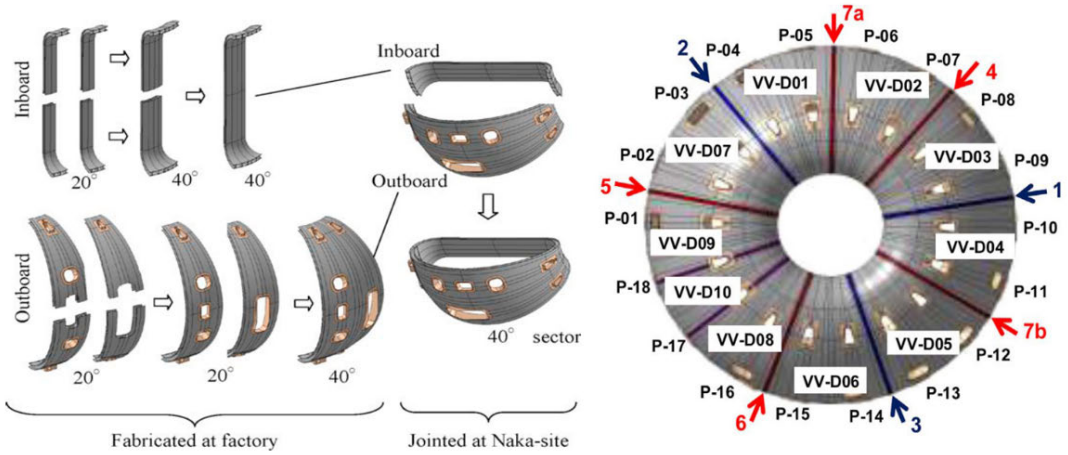

FIGURE 2. JT-60SA VV sector assembly at factory and on-site (left) and the whole VV assembly sequences (right).

in related literature [25]–[27], dynamic manipulability in related literature [25], dynamic force in such literatures [28] and [29], energy consumption in literature [30]. Based on built objective functions, multi-objective optimization can be usually done by setting different design variables of the parallel mechanism; the design variables can be the length of a limb, the diameters of the platforms and the angles between joints and links depend on different parallel robot configurations. In one piece of literature [24], the optimization based on workspace and stiffness was carried out, and in three pieces of literatures [30]–[32] in particulars, the optimizations based on force and torque indexes derived from the dynamic model is performed. In the multi-objective optimization, different algorithms were developed, the non-dominated sorting genetic algorithm II (NSGA-II) introduced in literature [33] was widely used in different research mentioned above as the optimization algorithm due to its low computation complexity and elitist strategy compared with traditional multi-objective evolutionary algorithms (EAs).

C. SCOPE

Despite different robot systems having been proposed by different researchers in various fields, the better solution is always attractive, especially in a mega project such as a fusion reactor development, where all kinds of systems interact with one another, there is a lack of robot system and robotic technology in fusion reactor environment. Currently, most of the parallel mechanisms have been designed in a small scale and the application required fast movement speed and accuracy, such as in the lifting application. The series mechanism can handle a heavy task, but the robot system is usually huge and must be mounted on the ground. In different fusion reactors, the welding sequence, welding technology, and tokamak environments are different. Therefore, a more dexterous mobile parallel robot is proposed in this paper, which is compact in structure, has less space required, is easy to evacuate, capable of carrying out a machining process with ± 0.1 mm machining accuracy. Furthermore, task-orientated multi-objective optimization of the parallel mechanism is carried out, and the results are compared with single-objective optimization. The proposed robot system can be adopted in different fusion reactors and other scenarios.

The remainder of the paper is organized as follows: in section II, the configuration of the dexterous mobile parallel mechanism is introduced, followed by kinematic and dynamic models derived from a geometric model. Section III formulates several objective functions based on the parallel robot machine purpose. And multi-objective optimization

simulations are implemented in section IV. Finally, conclusion and analysis are given in section V.

II. CONFIGURATION, KINEMATIC, AND DYNAMIC MODELS

In this section, firstly, the configuration of the newly designed dexterous mobile parallel mechanism is introduced, the main components are described, and the mechanism's working principle is introduced. Subsequently, the kinematic model and the dynamic model are derived.

A. CONFIGURATION

The proposed robot system consists of a parallel mechanism, carriage, and single-track rail shown in Figure.3. The newly designed single-track rail shown in Figure.4 is mounted on the VV inner wall, compared to the double-track rail proposed in [10], the newly designed single-track rail occupies less space on the inner wall, and the shape of the rail can easily be redesigned for other fusion reactor. There are four sub-rails on the single-track rail, the flat-wheel rail and the V-shaped rail are for the two wheels in the driven unit; they work together to constrain the carriage movement on the path without any shift in horizontal direction. The encoder rail is for the encoder gear mounted on the carriage to record the robot's movement. And the gear rail is for the gear driven by the electric servo motor with a speed reducer, in this way, high torque can be transmitted to the driving gear. In this configuration, two driven units are adopted to provide enough torque to drive the whole robot system. In the carriage shown in Figure.4, the adaptive compensation system is designed by connecting two driven units by gas springs, to eliminate the backlash caused by assembly error and movements. Because the driven unit must clamp the rail tightly even when the robot system moves to the bending position of the rail. Figure.5 shows the robot system positions on a straight segment and a bending segment on the rail, the distance between the two wheels on the bottom changes when the carriage moves into different positions, and they must have contact with the bottom side of the rail. Then the evacuate unit is designed for assembly convenience, the bottom part of the evacuate unit is bolted to the upper part so that even when the robot system is on the track rail, it is easy to disassemble the robot system, which is quite important if there is blackout in the system. This evacuation system allows the robot to be evacuated conveniently from the rail in any position fast, instead of disassembling the robot system piece by piece. The whole robot system on the rail mounted on the inner wall of the VV is shown in Figure.6, there are two splice plates marked in the figure and they are used for the joint adjacent VV sectors, compared with direct butt welding, splice plate welding is more suitable in compensating for considerable misalignment during the large component assembly, especially when large shrinkage of the welding exists. The splice plate assembly technology used in the VV assembly is:

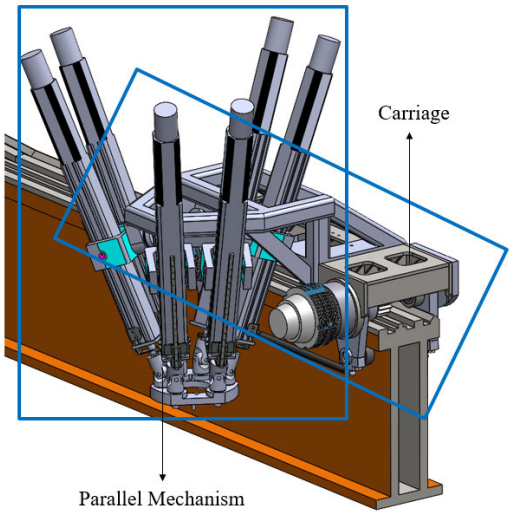

FIGURE 3. Mobile parallel mechanism on the track rail.

1) The rail is mounted on the inner wall of the VV sector, then the robot system is transported in. In ITER, the splice plate has thickness of 60 mm, and weighs more than 100 kg, a heavy-duty lift is installed on the end effector of the proposed robot system, to lift the splice plate and transport it to position;
2) Then the welding process starts on the splice plate from the outer wall to the inner wall in the sequence, a suitable fixture must be installed during the welding process to ensure the welding quality. The welding process should be performed continuously by driving the carriage on the rail;
3) The milling process will be carried out after the welding processes, during the process, it is proposed that the robot system execute segment by segment, which means the carriage carries the parallel mechanism to a position, then the parallel mechanism will move independently to perform the milling process; in this way, the milling accuracy is within ± 0.1 mm, and the parallel mechanism is able to reach any position in a 200 mm $\times$ 200 mm $\times$ 300 mm cube.

B. GEOMETRIC MODEL

The 6-DoF parallel mechanism in Figure.3 mainly consists of a fixed platform, a movable platform, six prismatic actuators and 12 universal joints. The universal joints on the top side are connected with the actuator in the middle position of the actuator by side trunnion attachments. This configuration allows the robot to move through the port and allow full-stroke movements of the actuators to reach more workspace. The simplified geometry and the views of a fixed platform and movable platform are shown in Figure.7. The fixed platform B and the movable platform A are linked by 12 universal joints represented by a_i $(i = 1, 2, 3, 4, 5, 6)$ on a movable platform located on the circle of diameter D, b_i $(i = 1, 2, 3, 4, 5, 6)$

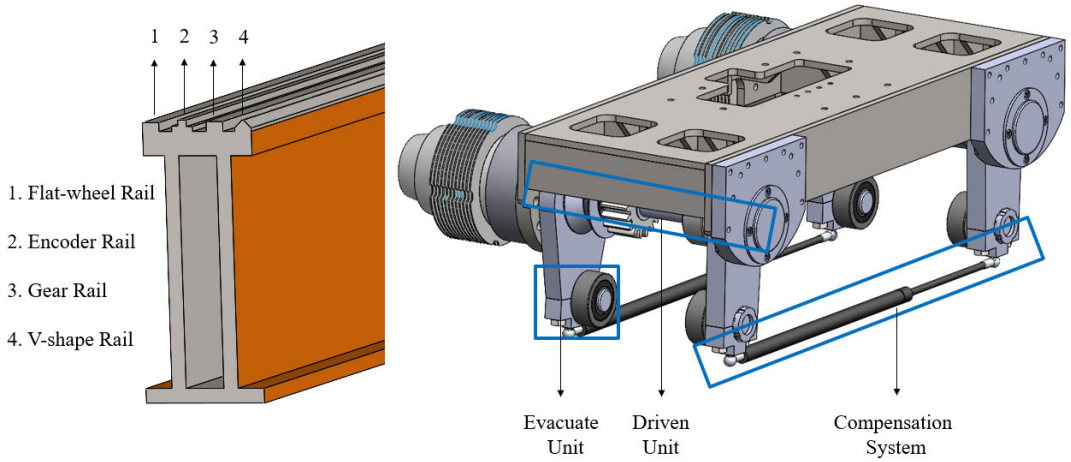

FIGURE 4. Single-track rail and its cross section (left) and carriage (right).

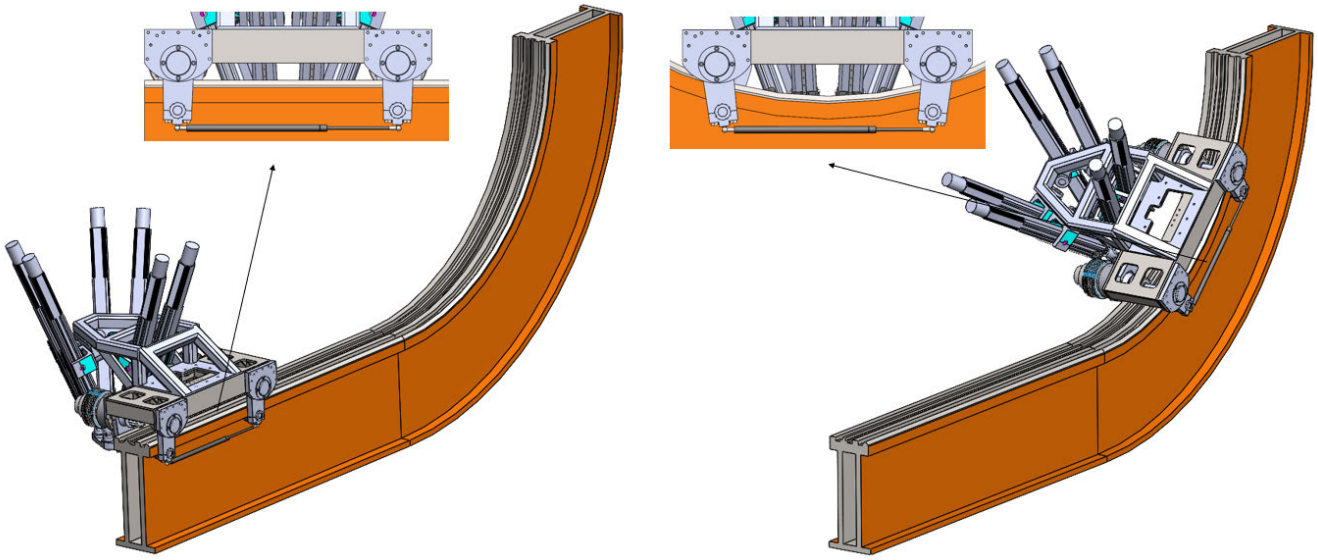

FIGURE 5. Robot system on straight segment (left) and bending segment (right) of the rail.

on a fixed platform located on the circle of diameter d and actuators represented by l_i $(i = 1, 2, 3, 4, 5, 6)$.

C. KINEMATIC MODEL

According to Figure.7, the distance vector of each limb is obtained in Eq.(1) and the Jacobian matrix is determined in Eq.(2):

$$l_i\hat{s}_i = {}^{A}P + {}^{A}R_B b_i - a_i \tag{1}$$

$$J = \begin{bmatrix} \hat{s}_1^T & (b_1 \times \hat{s}_1)^T \\ \hat{s}_2^T & (b_2 \times \hat{s}_2)^T \\ \vdots & \vdots \\ \hat{s}_6^T & (b_6 \times \hat{s}_6)^T \end{bmatrix} \tag{2}$$

where l_i is the length of the ith limb, $\hat{s}_i$ is the unit vector of the limb, ${}^{A}P = [px\ py\ pz]^T$ and ${}^{A}R_B$ are the position vector and orientation of point O_A, a_i and b_i denote the points on the movable and fixed platform with respect to their own frame, respectively. The Jacobian matrix J is a 6×6 square matrix, and it can be further derived to dexterity and manipulability objective functions, for example.

D. DYNAMIC MODEL

The closed-form dynamic formulation introduced in related literature [13] are used here to simulate the dynamic behavior of the parallel mechanism. The actuator dynamic forces are calculated from Eq.(3).

$$\tau = J^{-T}\left(M(\mathcal{X})\ddot{\mathcal{X}} + C(\mathcal{X}, \dot{\mathcal{X}})\dot{\mathcal{X}} + G(\mathcal{X}) + \mathcal{F}_d\right) \tag{3}$$

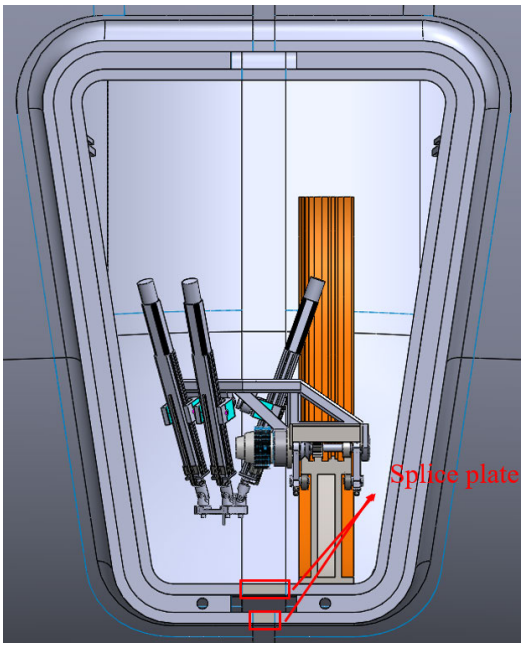

FIGURE 6. Robot system on the rail mounted on the inner wall of VV.

TABLE 1. Abbreviation of the model.

Abbreviation	Meaning
τ	Actuator force of limbs
M	Mass matrix
C	Coriolis and centrifugal matrix
G	Gravity factor
$\mathcal{F}_d$	External wrench
$\mathcal{X}$	Position of center point of movable platform
$\dot{\mathcal{X}}$	Velocity of the center point of movable platform
$\ddot{\mathcal{X}}$	Acceleration of a center point of a movable platform
J	Jacobian matrix
$l_i (i = 1, 2, \ldots, 6)$	Length of ith limb
$\hat{s}_i (i = 1, 2, \ldots, 6)$	Unit vector of the ith limb
A_P	Position vector of center of movable platform
A_B^R	Rotation matrix
a_i	Position of a_i with respect to frame $\{A\}$
b_i	Position of b_i with respect to frame $\{B\}$
$[\cdot]_\times$	Skew-symmetric matrix of vector $[\cdot]$
I_{xx_i}	Equivalent moment of inertia in x and y directions
g	Gravitational constant
c_{i1}	Half-length of cylinder
c_{i2}	Half-length of piston
m	Mass of movable platform
m_{i1}	Mass of cylinder
m_{i2}	Mass of piston
D	Diameter of fixed platform
d	Diameter of movable platform
α	Angle on fixed platform
β	Angle on movable platform

where $M(\mathcal{X})$ is the mass matrix, $C(\mathcal{X})$ is the Coriolis and centrifugal matrix, $G(\mathcal{X})$ is the gravity vector and $\mathcal{F}_d$ is the external force and torque. The mass matrix $M(\mathcal{X})$ defines the kinetic energy of the system and is derived from Eq.(4) to Eq.(9):

$$M(\mathcal{X}) = M_p + \sum_{i=1}^{i=6} M_{li} \tag{4}$$

$$M_p = \begin{bmatrix} mI_{3\times3} & 0_{3\times3} \\ 0_{3\times3} & {}^{A}I \end{bmatrix}_{6\times6} \tag{5}$$

$$M_{li} = J_i^T M_i J_i \tag{6}$$

$$J_i = \begin{bmatrix} I_{3\times3} & -b_{i\times} \end{bmatrix} \tag{7}$$

$$M_i = m_{i_2}\hat{s}_i\hat{s}_i^T - \frac{1}{\ell_i^2} I_{xx_i}\hat{s}_{i\times}^2 - m_{c_e}\hat{s}_{i\times}^2 \tag{8}$$

$$m_{c_e} = \frac{1}{\ell_i^2}\left(m_{i_1}c_{i_1}^2 + m_{i_2}c_{i_2}^2\right) \tag{9}$$

The Coriolis and centrifugal matrix $C(\mathcal{X})$ includes inertial forces caused by the Coriolis and centrifugal accelerations, which is derived from Eq.(10) to Eq.(14):

$$C(\mathcal{X}, \dot{\mathcal{X}}) = C_p + \sum_{i=1}^{i=6} C_{li} \tag{10}$$

$$C_p = \begin{bmatrix} 0_{3\times3} & 0_{3\times3} \\ 0_{3\times3} & \omega_\times {}^{A}I_p \end{bmatrix}_{6\times6} \tag{11}$$

$$C_{li} = J_i^T M_i \dot{J}_i + J_i^T \mathcal{C}_i J_i \tag{12}$$

$$C_i = -\frac{2}{\ell_i} m_{c0}\dot{\ell}_i\hat{s}_{i\times}^2 - \frac{1}{\ell_i^2} m_{i_2}c_{i_2}\hat{s}_i\dot{x}_i^T\hat{s}_{i\times}^2 \tag{13}$$

$$m_{c_o} = \frac{1}{\ell_i} m_{i_2}c_{i_2} - \frac{1}{\ell_i^2}\left(I_{xx_i} + \ell_i^2 m_{c_e}\right) \tag{14}$$

The gravity vector $G(\mathcal{X})$ defines the gravity of the system and it is derived from Eq.(15) to Eq. (19):

$$G(\mathcal{X}) = G_p + \sum_{i=1}^{i=6} G_{li} \tag{15}$$

$$G_p = \begin{bmatrix} -mg \\ 0_{3\times1} \end{bmatrix}_{6\times1} \tag{16}$$

$$G_{li} = J_i^T G_i \tag{17}$$

$$G_i = \left(m_{g_e}\hat{s}_{i\times}^2 - m_{i_2}\hat{s}_i\hat{s}_i^T\right) g \tag{18}$$

$$m_{g_e} = \frac{1}{\ell_i}\left(m_{i_1}c_{i_1} + m_{i_2}\left(\ell_i - c_{i_2}\right)\right) \tag{19}$$

The external force and torque $\mathcal{F}_d$ is a 6×1 matrix defines the forces and torques applied to the center point of the movable platform. Some abbreviations are listed in Table.1.

Then the same parameters and trajectory mentioned in literature [13] are used here to check whether the model has been built successfully, the calculated dynamic forces of the six actuators illustrated in Figure.8 are exactly the same as those in the reference. This shows that the dynamic model is successfully built.

The machining process of IWR for ITER was introduced in referenced literature [10]; here the same machining force is adopted and is illustrated in Figure.9. The calculated peak machining force $\mathcal{F}_d$ of 650 N is used in the further calculation as external force.

III. OBJECTIVE FUNCTIONS

Multi-objective optimization can involve many objective functions, the choice of objective functions should be based on application, in referenced literature [24], stiffness and

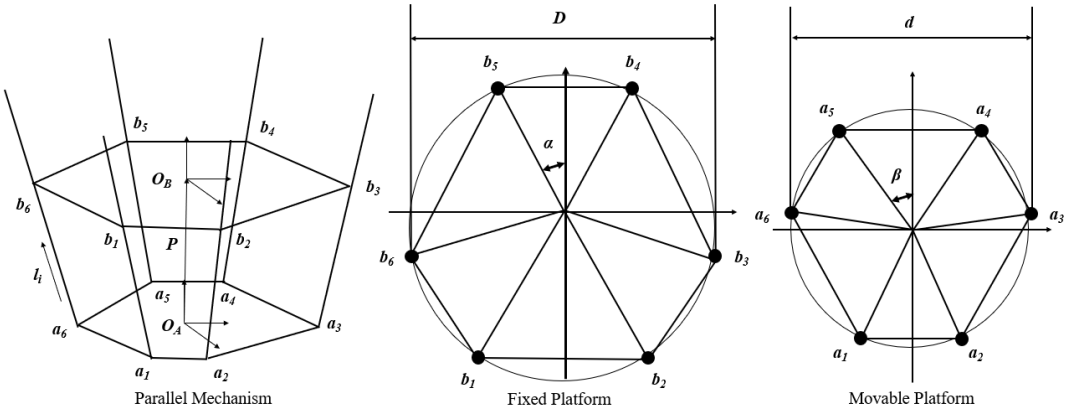

FIGURE 7. Parallel mechanism kinematic model, fixed platform and movable platform views.

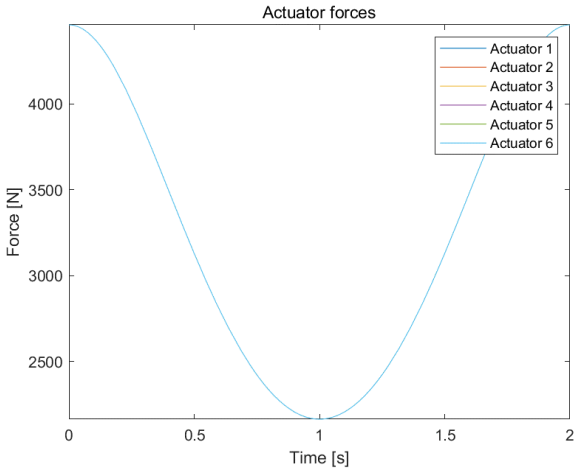

FIGURE 8. Six actuator forces along the predefined trajectory.

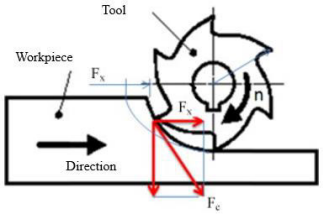

FIGURE 9. Cutting force during the machining process.

workspace are considered, in referenced literature [34] dexterity and manipulability are considered, in pieces of referenced literature [30]–[32], force and torque are considered. All of these objective functions are derived from the kinematic and dynamic models. Based on how the objective functions are derived, they can be divided into static-based objective functions and dynamic-based objective functions.

In order to optimize the parallel mechanism performance throughout the whole workspace, global objective function should be derived on the base of local objective functions instead. In this situation, the workspace is not only an objective function, but also a way to be used to build global objective function. In static-based optimization, usually the workspace can be calculated by different methods, such as discrete-boundary-searching algorithm, Monte Carlo random search method, exhausted search method and representative points method [20], [24], [35]–[37]. In dynamic-based optimization, model properties such as mass, inertia, and acceleration must be considered, so several trajectories are usually selected to simulate the real operations, which were mentioned in literatures [38] and [39]. In this section, three objective functions are introduced to represent the overall behavior of the parallel mechanism.

A. GLOBAL DYNAMIC FORCE INDEX

Since this proposed robot system is mainly used for welding and machining processes, and force and accuracy requirements on the welding process is much smaller than that of machining process. The absolute minimum dynamic force and maximum dynamic force among the six actuators are denoted as τ_{min} and τ_{max}. To ensure that force's distribution on each actuator is relatively similar, the difference between τ_{min} and τ_{max} should be minimized, so the dynamic force index is defined as the standard deviation of the τ and it is written in Eq.(20), where $D(\cdot)$ represents the standard deviation of the elements in the matrix and the global dynamic force index in work space W is expressed in Eq.(21).

$$DFI = D(\tau)/\tau_{max} \tag{20}$$

$$GDFI = \frac{\int_W DFI dW}{\int_W dW} \tag{21}$$

B. GLOBAL DYNAMIC DEXTERITY INDEX

Dexterity index (DI) is derived from the Jacobian matrix and denoted in Eq.(22):

$$DI = -1/\kappa = -1/\|J\| \left\|J^{-1}\right\| \tag{22}$$

where $||\cdot||$ denotes the norm of the matrix. The condition number κ is a value between 1 and infinity, and the isotropic

configuration is obtained when $\kappa = 1$. As a result, *DI* should be kept as small as possible for better performance. The dynamic dexterity index (*DDI*) put the mass matrix $M(\mathcal{X})$ into *DI* and it correspond to the ability of the structure to drive the movable platform for a given configuration at zero velocity, the *DDI* is denoted in Eq.(23), where $\sigma_{max}(M)$ and $\sigma_{min}(M)$ are the maximum and minimum eigenvalues of the mass matrix M and it should be kept as small as possible. Additionally, the global dynamic dexterity index (*GDDI*) is denoted in Eq.(24).

$$DDI = -1/\kappa_D = -\frac{\sigma_{\min}(M)}{\sigma_{\max}(M)} \tag{23}$$

$$GDDI = \frac{\int_W DDI dW}{\int_W dW} \tag{24}$$

C. GLOBAL STIFFNESS INDEX

The stiffness affects the parallel mechanism accuracy and ability to resist deformation directly, the local stiffness of the mechanism can be simplified to Eq.(25) when all the actuators are treated as springs and they have the same stiffness coefficient k. Referenced literature [40] built a stiffness model of hybrid robot, which has similar joints and links of the proposed parallel mechanism, the stiffness of the whole robot is obtained as $K = C^{-1}$, where C is the compliance matrix. The maximum eigenvalues of matrix $(K^{-1})^T K^{-1}$ is calculated and the local stiffness matrix is defined in Eq.(26), and it is further derived into the global stiffness index (*GSI*) in Eq.(27).

$$K = kJ^T J \tag{25}$$

$$LSI = \sqrt{\max(eig\left(\left|(K^{-1})^T K^{-1}\right|\right))} \tag{26}$$

$$GSI = \frac{\int_W LSI dW}{\int_W dW} \tag{27}$$

IV. MULTI-OBJECTIVE OPTIMIZATION

In this section, the single-optimization and multi-optimization methods are firstly introduced, then optimization problems are set up, finally, the optimization results are shown in the end.

A. OPTIMIZATION METHOD

Different multi-objective evolutionary algorithms (MOEAs) are used in various of optimization problems. NSGA-II introduced in literature [33] is selected as the optimization method and the procedure of NSGA-II illustrated in Figure.10. A genetic algorithm can be simplified into four stages:

1) Generation: when t=1, generate N solutions to form the first population P_1, the fitness of solutions is evaluated;
2) Crossover, mutation and evaluation: generate offspring population Q_t and mutate each solution in Q_t with mutation rate, then the fitness of solution in Q_t is evaluated;
3) Selection: population of size N from Q_t are selected, and they are assigned as next generation population Q_{t+1};

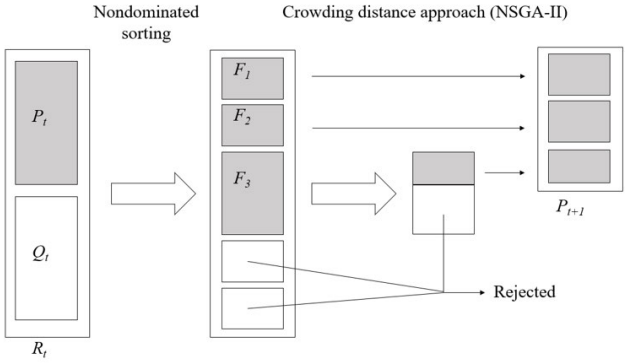

FIGURE 10. NSGA-II procedure.

4) End: the algorithm ends once predefined termination criterion is met.

The procedure of NSGA-II differs from GA in the selection stage, NSGA-II introduces the crowded-distance approach, which can estimate the density of solutions surrounding a certain particular solution in the population; in this way, not only does the complexity of the computation decrease, but it can also maintain the spread of solutions. In NSGA-II, instead of selecting population of size N from Q_t, firstly, a population of size $2N$ is formed as R_t by combining population P_t and Q_t, then a population of size N from R_t is ranked according to its value. Now, the best solution in set F_1 is firstly chosen, and then F_2, but in Figure.10, the example shows that once F_3 is fully chosen, the size of P_{t+1} is more than that of N. So a certain amount of population in F_3 is chosen and put into P_{t+1} based on the crowded-distance approach. The basic idea of the crowded-distance approach shown in Figure.11 is firstly to locate two points $i-1$ and $i+1$ on both sides of the point i, then the perimeter of the cuboid surrounded by these two points are estimated, which is called crowding distance. After that, the solution with smaller crowding distance means that more solutions are generated in this area. Finally, the solutions with better rank in the population and lower crowding distance are selected to fill the next generation until the size of the population is equal to N. However, with the increasing of the objectives, the dimension of the problem increases, and the performance of NSGA-II decreases, as a result, optimization results are promising with respect to 2-3 objectives. For a more objective optimization method, a many-objective optimization should be studied, such as NSGA-III, which was introduced in literature [41].

B. GLOBAL OPTIMIZATION METHOD

If the optimization problem is only related to the kinematic model, global optimization is achieved by calculating the objective function values in different positions uniformly distributed inside the whole workspace, the time spent and calculation accuracy are based on the amount of defined positions. The procedure of the calculation can be summed up in the following stages:

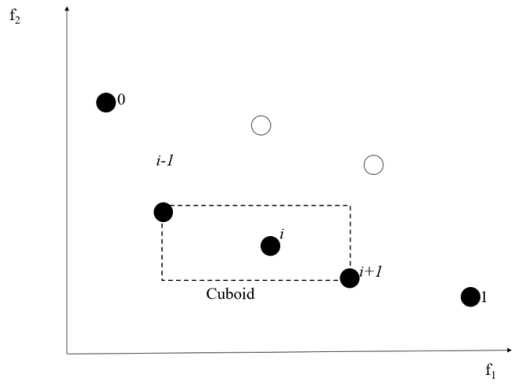

FIGURE 11. NSGA-II crowded-distance approach.

1) Local objective function value is calculated in certain position of the structure configuration;
2) Workspace is evaluated. Certain amounts of points are uniformly collected in the workspace based on a pre-defined calculation accuracy requirement. In referenced literature [34], the amounts of points in workspace were decided by using relative error constraints. A discrete-boundary-searching algorithm to decide the amount of points in workspace was used in referenced literature [20]. Another method introduced in referenced literature [37] selected a certain amount of points by using the Monte Carlo method;
3) Global objective function value is calculated concerning all the points in the workspace, which is usually the average value of the objective functions in all the positions.

The global optimization method mentioned above is suitable for static optimization, which evaluates the performance of the structure in certain positions above the workspace. However, in structure dynamic performance optimization, the dynamic forces and torques are highly affected by structure inertia, friction, and external disturbance. So, trajectory-based global optimization is better than the workspace-volume-based global optimization. And the movement of the parallel mechanism can be simulated. In literature [39], optimization of a parallel robot for pick-and-place application in a predefined workspace using different trajectories were studied, in literature [42], an S-shape trajectory was defined to study the robot's behavior in the milling process. The robot system introduced in this paper will carry out the both welding and milling process, in welding process, the accuracy is required to be controlled within ±0.5 mm, in the milling process, the requirements are higher, the accuracy should be controlled within ±0.1 mm. To simulate the milling process, the trajectory must be designed to let the mechanism move continuously and smoothly, and acceleration of the robot should also be involved. During the milling process, the carriage will stop in position and the parallel mechanism will carry out tasks in a cube of 200 mm×200 mm×300 mm. The speed of the milling process is set as 1 mm/s. And since

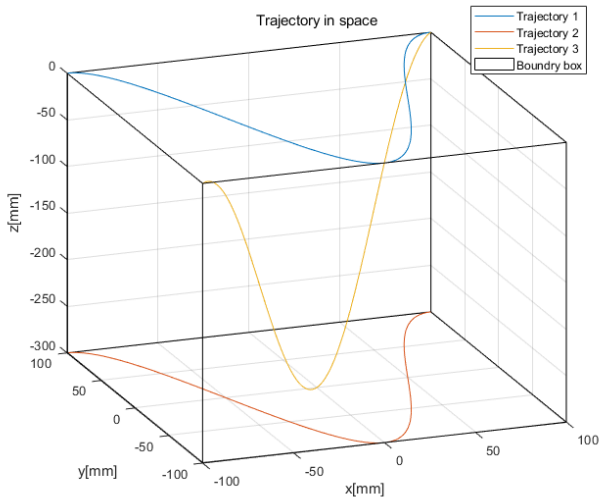

FIGURE 12. Trajectories applied in the optimization simulation.

TABLE 2. Design variables ranges.

Design variables	Original	Ranges
D	$1.0[m]$	$1.0 < D \leqslant 1.5[m]$
d	$0.5[m]$	$0.2 < d \leqslant 0.6[m]$
α	$20[^\circ]$	$10 < \alpha \leqslant 55[^\circ]$
β	$48[^\circ]$	$10 < \beta \leqslant 55[^\circ]$

the task is different from other parallel mechanisms, such as lifting and sorting, where acceleration is highly demanding, the functions of three trajectories $P_i(t), (i = 1, 2, 3)$ are designed for this parallel mechanism, and formulated with respect to time t, denoted in Eq.(28), Eq.(29), and Eq.(30), the illustration of these three trajectories is shown in Figure.12.

$$P_1(t) = \begin{bmatrix} x_1(t) = t - 100 \\ y_1(t) = 100 * \sin\left(\frac{\pi}{100} * t + \frac{\pi}{2}\right) \\ z_1(t) = 0 \end{bmatrix} \tag{28}$$

$$P_2(t) = \begin{bmatrix} x_2(t) = t - 100 \\ y_2(t) = 100 * \sin\left(\frac{\pi}{100} * t + \frac{\pi}{2}\right) \\ z_2(t) = -300 \end{bmatrix} \tag{29}$$

$$P_3(t) = \begin{bmatrix} x_3(t) = t - 100 \\ y_3(t) = t - 100 \\ z_3(t) = -150 + 150 * \sin\left(\frac{\pi}{100} * t + \frac{\pi}{2}\right) \end{bmatrix} \tag{30}$$

C. DESIGN VARIABLES

The variables D, d, α, β are used as design variables. After taking workspace requirements, components movement limitations, and robot system movement in the vacuum vessel into consideration in the simulation software, the design variables boundaries are estimated from kinematic simulation results and shown in Table.2. In addition, the constraint α<β is set.

D. OPTIMIZATION SETUP

The flow chart of the optimization setup is shown in Figure.13.

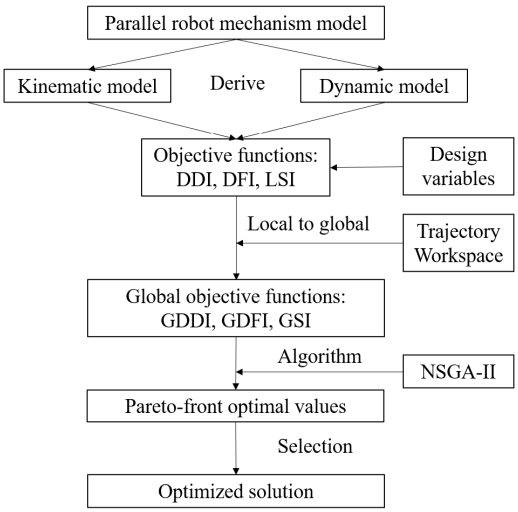

FIGURE 13. Multi-objective optimization problem setup flow chart.

TABLE 3. Group set up for comparison.

	Algorithm	Objective functions		
Group 1	GA	DI	FI_1	$-SI_1$
Group 2	NSGA-II	DI	FI_1	$-SI_1$
Group 3	GA	DI	FI_2	SI_2
Group 4	NSGA-II	DI	FI_2	SI_2
Group 5	GA	DI	FI_1	$-SI_1$

1) The kinematic and dynamic models of the parallel mechanism are derived;
2) Design variables are carefully decided based on the tasks, and objective functions involving design variables are decided and derived;
3) Trajectories or the workspace is defined, and global objective functions are formulated;
4) NSGA-II is selected as the optimization algorithm, and optimization program is set up;
5) The Pareto-front optimal values are extracted from the optimization;
6) The optimized solutions are selected from the solutions pool.

There are also several pieces of literature about single-objective optimization of the parallel mechanism, where a cost function combines different objective functions allocated by different weights is introduced, the general cost function formulation can be seen in Eq.(31), where $x = [D, d, \alpha, \beta]$, and w_n is the weight coefficient allocated to each objective function f_n.

$$f(x)_{single} = w_1 * f_1 + w_2 * f_2 + \ldots + w_n * f_n \qquad (31)$$

In this way, the optimization can also be seen as single-objective multi-variable optimization, the goal of which is to minimize the single-objective $f(x)$ and multi-variables are $w_n * f_n$. Once the number of the optimization iteration reaches the specified value or the calculation accuracy reaches the pre-assigned requirement, the optimization process stops, and the actual design variables x values are extracted. Therefore, it can be noticed that the adjustments on the weights w_n is vital in this optimization method, and it can decide how the different objective functions are balanced. Otherwise, when $f_n(n = 1, 2, \ldots n)$ are close in numerical value, if more weight w_1 is allocated to f_1, the objective function f_1 contributes more to the cost function, and affects the optimization result. Therefore, if w_n is not chosen carefully based on the behaviour of each objective function, the optimization problem turns toward being single-objective single-variable optimization. However, if the optimization is not complicated, designer can adjust the weight factor w_n to get optimal results based on tasks that parallel mechanism carries out. In referenced literature [43], a cost function of stiffness was built in each direction, and optimization on a 5-DoF tripod parallel robot machine with gantry system was performed. In literature referenced [22], the weight factor was not used, instead, the cost function was built by multiplying stiffness and volume. In referenced literature [44], optimization using different weights on objective function was carried out. The algorithms used in the single-objective optimizations are mainly a genetic algorithm, differential evolution, and particle swarm optimization.

However, the drawbacks of the single-objective optimization must be noted. Firstly, the cost function value will be evaluated and the solution with tbe smaller value will be reserved. Secondly, the cost function is the sum of different objective functions, the normalization is troublesome, and it must be carefully tuned; for example, the force, the stiffness and the dexterity have huge differences in numerical values, and if the calculated objective function values are not distributed evenly in the work space, the normalization is more complicated, in another word, the result might be locally optimized instead of globally optimized. Thirdly, the weights allocation determines the priorities of the objective functions, if the weights are not decided carefully, the results may not be reliable. However, in many literatures mentioned above, there is lack of introduction of how the normalization method works or how the weights are selected in a reasonable way. However, in multi-objective optimization, there is no need to normalize the objective function or put weight on objective functions. So next, a single-objective optimization is set as an example to compare the optimization results using two different optimization methods. Firstly, five objective functions are introduced covering dexterity, force, and stiffness. DI is the dexterity index, FI_1 is the maximum reaction force among the six actuators, FI_2 is the standard deviation of the reaction forces of the six actuators, SI_1 is the mean value of the diagonal elements in stiffness matrix K, and SI_2 is the standard deviation value of the diagonal elements in stiffness matrix K. The optimization goal is to minimize the value of objective function, then the negative value of $-SI_1$ is adopted. Five groups are set up in Table.3 to compare the optimization result using single-objective optimization and multi-objective optimization, genetic algorithm is selected as the single-objective optimization algorithm.

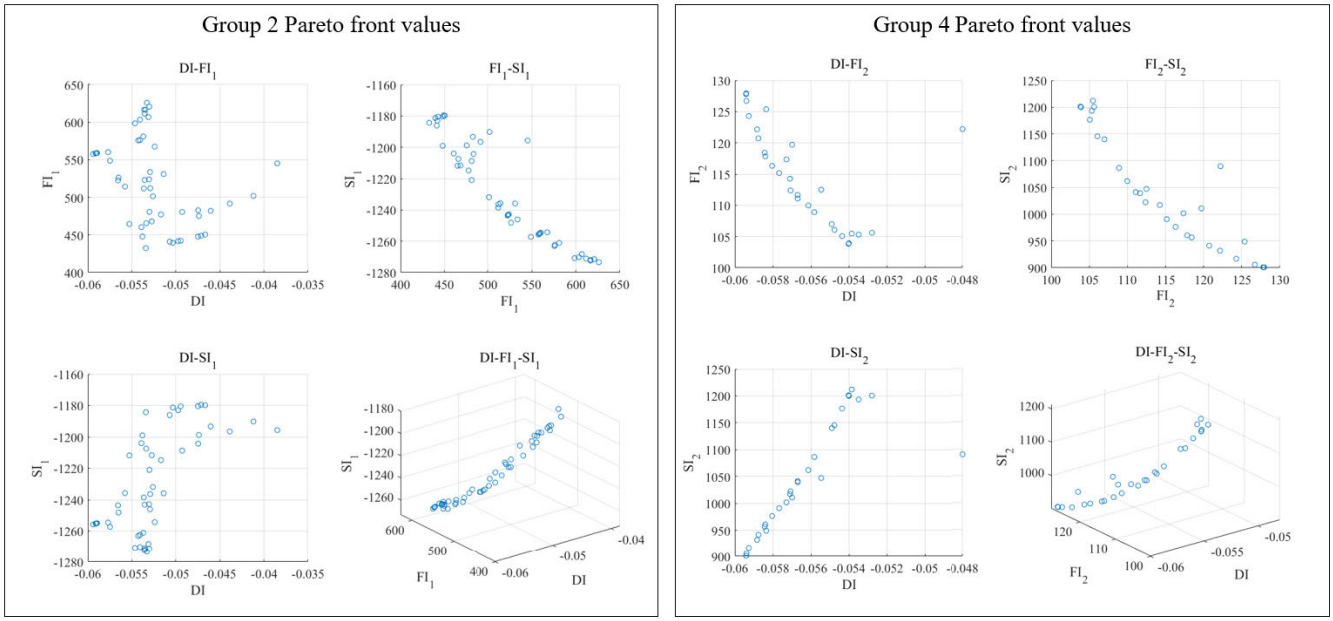

FIGURE 14. Group 2 and group 4 Pareto-front values.

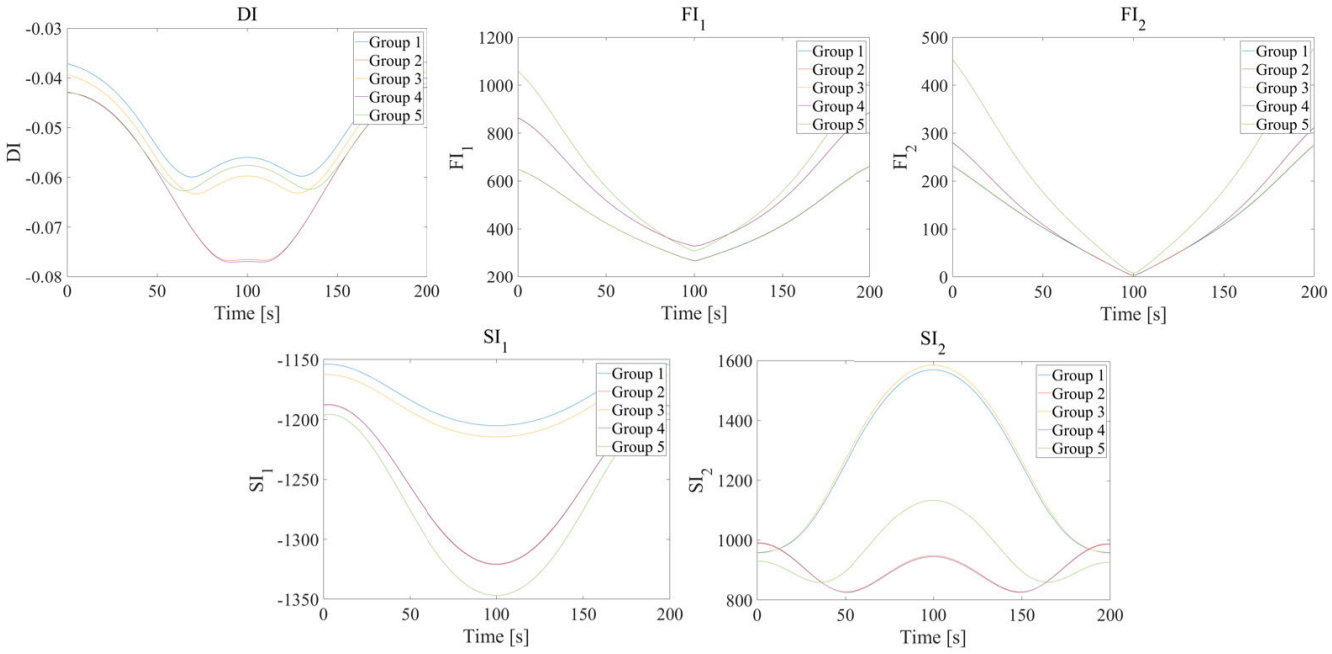

FIGURE 15. Results comparison between 5 groups.

The trajectory P_3 is used here to set up the global optimization, in normalization, each objective function value along the trajectory is calculated, then considering the mean value, the median value, and the standard deviation value, they are normalized. In group 1, the normalization factors are [100,0.004,0.002] for DI, FI_1, and SI_1, respectively. In group 3, the normalization factors are [100,0.02,0.002] for DI, FI_2, and SI_2. The weights [1,1,1] are equally allocated in each objective function, in this way, the cost function treats all the objective functions equally. To show the difference when different weights allocated on objective functions, group 5 is set, the objective functions in group 5 are DI, FI_1, and SI_1, the weights are [1,0.1,1] on each objective function, respectively.

E. OPTIMIZATION RESULTS

In the comparison between single-objective optimization and multi-objective optimization, the Pareto-front values of groups 2 and 4 adopting NSGA-II are shown in Figure.14, the mean value of the optimal solutions are calculated, and the results of five groups are shown in Table.4. Then the objective

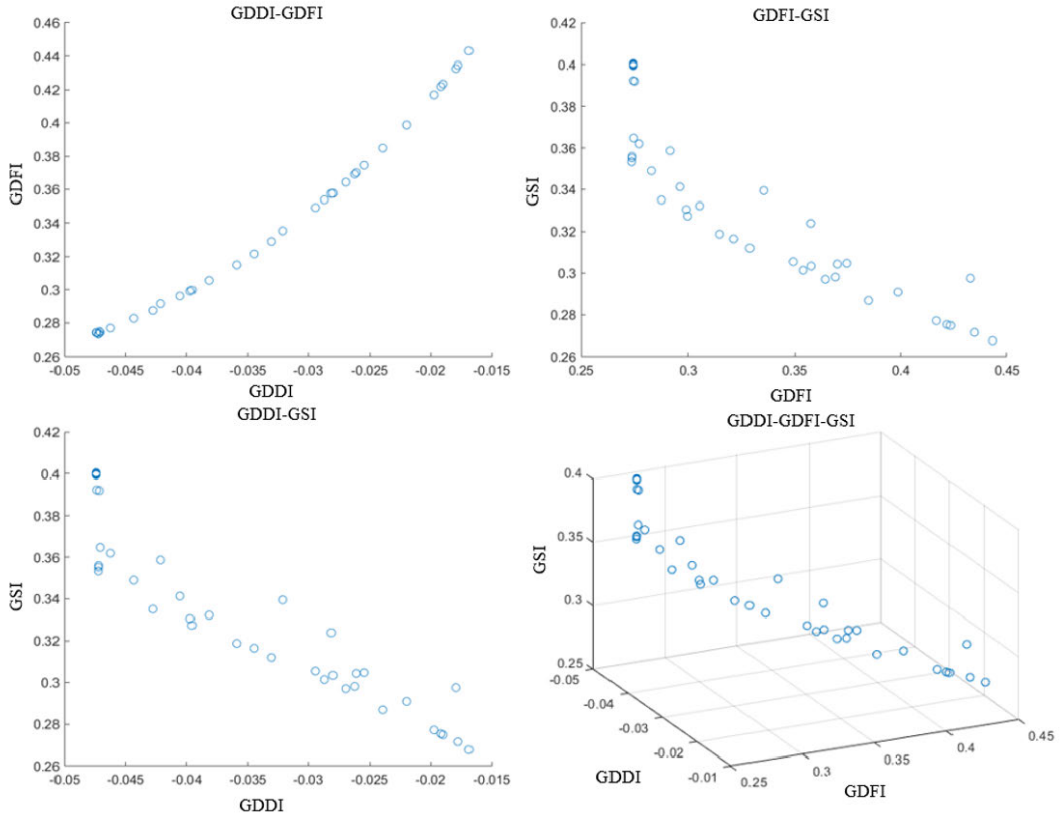

FIGURE 16. Optimization Pareto-front optimal results.

function values of DI, FI_1, FI_2, SI_1, and SI_2 in each group are calculated and shown in Figure.15. The result indicates group 2 and 4 using NSGA-II as optimization algorithms are better than others, and the improvements are obvious. There is no clear difference between each in FI_1 values, however, due to less weight being put in FI_1 in group 5, the optimized results are worse than others. The standard deviation of actuator forces, FI_2 behaves similarly to FI_1. The SI_1 values in groups 2, 4, and 5 perform better, among which group 2 and group 4 adopt the NSGA-II algorithm. The results of SI_2 values indicate that group 2 and group 4 perform better. Compared to the original design, all the objective functions are improvements to different extents. To summarize, there are two findings, the first finding is that the multi-objective optimization (NSGA-II) has obvious advantages on this optimization problem compared with single-objective optimization. The second finding is that in single-objective optimization, the weights that are allocated to different objective functions have signification effects on the optimization results, and sometimes, the result may end up at local optimization and not be reliable.

Subsequently, when taking the three trajectories as a global optimization method, after the simulation, 50 sets of optimized solutions are extracted, then corresponding objective function values and Pareto-front graphs are shown in Figure.16. In theory, all the solutions are feasible, however,

TABLE 4. Group set up for comparison.

	$\alpha\,(^\circ)$	$\beta\,(^\circ)$	D(m)	d(m)
Group 1	10.2825	56.3582	1.0029	0.5758
Group 2	10.0905	59.9449	1.4969	0.5993
Group 3	11.3229	54.9985	1.0205	0.5999
Group 4	10.0099	59.9988	1.4999	0.5999
Group 5	18.1313	46.5609	1.4999	0.6000

TABLE 5. Optimized design variable values.

Design variables	Optimized	Original
D	$1.4961[m]$	$1.0[m]$
d	$0.5537[m]$	$0.5[m]$
α	11.692[°]	20[°]
β	57.855[°]	48[°]

to evaluate the solution among all the optimized solutions, a selection method is introduced here, each point in the 3D Pareto-front figure is a vector of [*GDDI GDFI GSI*], the norm of each point is calculated, which is the distance from this point to the origin point. The point with the lowest norm value is selected as the selected solution here. Then the corresponding optimized variable values and original values are shown in Table.5.

To compare the optimized results with the original results, six actuators' dynamic forces, *LSI*, *DDI*, and *DFI* along three trajectories in Eq.(28), Eq.(29), and Eq.(30) are calculated with original design variable values and optimized design

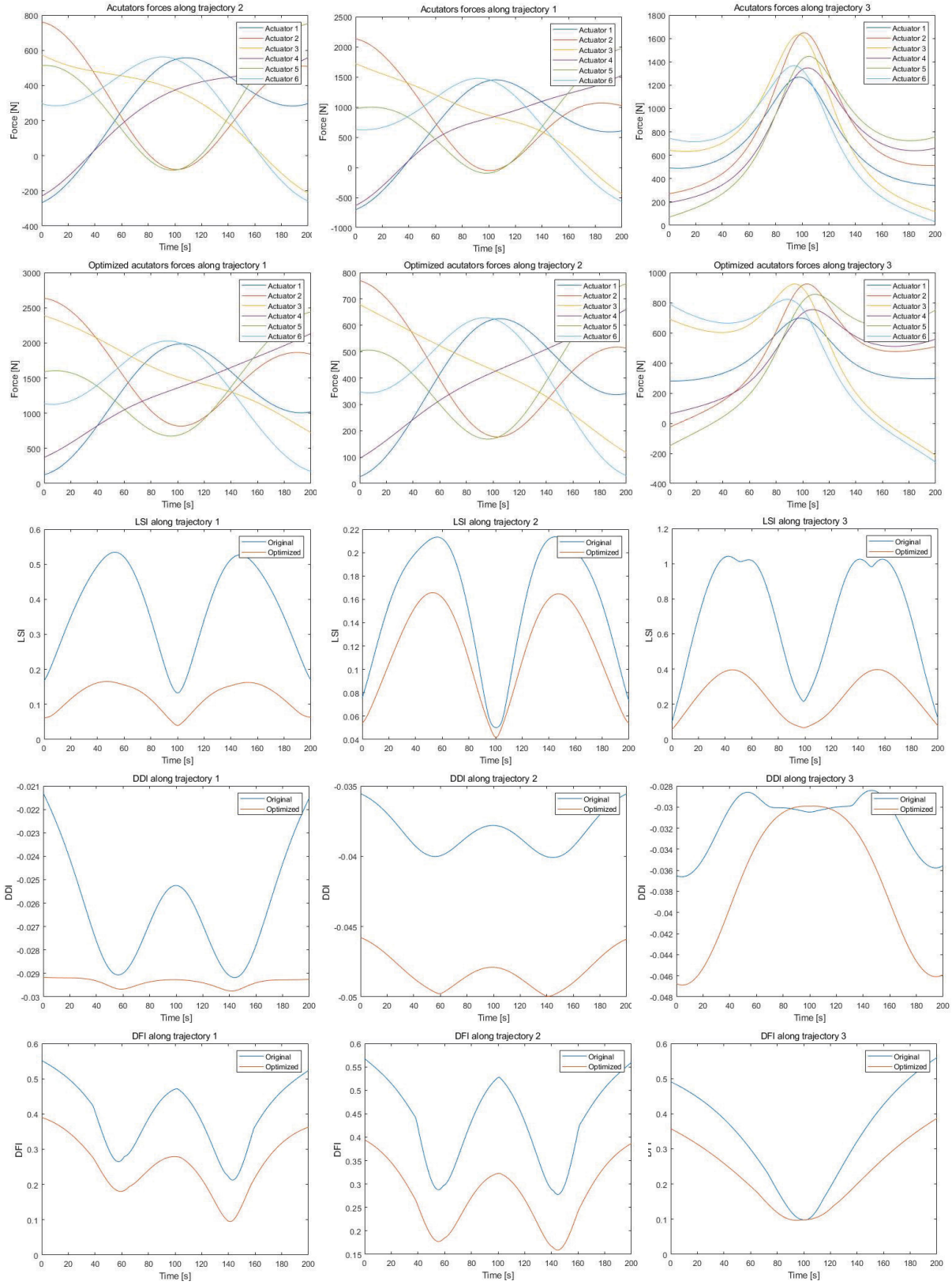

FIGURE 17. Comparison between original and optimized results.

FIGURE 18. Mobile parallel robot system in laboratory.

variable values, the results, which are shown in Figure.17. There are obvious improvements on each objective, however, in some local position, such as when $t = 50$, the value of *DDI* is a little bit smaller than the original result. However, over all, the optimization results are promising.

V. CONCLUSION AND DISCUSSION

This paper focuses on the research of development of a dexterous mobile parallel mechanism for a fusion reactor vacuum vessel assembly, compare this design with other robot machines, the proposed robot system has advantages including light weight, high mobility, high stiffness, ease of evacuation, the capability to carry out heavy-duty machining work, and ease of development for other fusion reactors. The robot system in Figure.18 was built, assembled and tested, welding and machining processes are performed, the robot system can achieve smooth automatic gas (tungsten inert gas welding and milling accuracy is within ± 0.1 mm), and the performance of the mechanism was validated and can be proposed to function in the fusion reactor environment. Furthermore, by changing the apparatus installed on the end effector, the robot system can carry out different tasks, such as inspection. Overviews of single-objective optimization and multi-objective optimization on parallel mechanisms are given, different objective functions are derived, which are also a guideline for future research. The global multi-objective optimization based on several objective functions of the parallel mechanism is carried out from a proposed parallel mechanism. There are quite many constraints in designing robot structure in a narrow fusion reactor environment, which highlights the importance of the multi-objective optimization. The optimized results are mapped to compare the performance of the original model and the optimized model, and the results reveal the success of the optimization simulation. This can help designers to develop robot structure for different purposes in different fields, especially for the design of fusion reactors of the future, where many components interact with each other, and many components are in the concept design phase, so the proposed mechanism will be beneficial from the applications and optimization can make the design process more efficient and accurate.

REFERENCES

[1] Y. Song, S. Wu, Y. Wan, J. Li, M. Ye, J. Zheng, Y. Cheng, W. Zhao, and J. Wei, "Concept design on RH maintenance of CFETR Tokamak reactor," *Fusion Eng. Des.*, vol. 89, nos. 9–10, pp. 2331–2335, Oct. 2014.

[2] M. Onozuka, J. P. Alfile, P. Aubert, J.-F. Dagenais, D. Grebennikov, K. Ioki, L. Jones, K. Koizumi, V. Krylov, J. Maslakowski, M. Nakahira, B. Nelson, C. Punshon, O. Roy, and G. Schreck, "Manufacturing and maintenance technologies developed for a thick-wall structure of the ITER vacuum vessel," *Fusion Eng. Des.*, vol. 55, no. 4, pp. 397–410, Sep. 2001.

[3] T. Brown, K. Kim, C. Kessel, G. H. Neilson, P. Titus, A. Zolfaghari, S. Baik, K. Im, H.-C. Kim, G.-S. Lee, Y.-S. Lee, S. Oh, and J.-H. Yeom, "Progress in developing the K-DEMO device configuration," in *Proc. IEEE 25th Symp. Fusion Eng. (SOFE)*, Jun. 2013, pp. 2–6.

[4] C. H. Choi *et al.*, "Status of the ITER vacuum vessel construction," *Fusion Eng. Des.*, vol. 89, nos. 7–8, pp. 1859–1863, 2014.

[5] Y. Shibama *et al.*, "Assembly technologies of the vacuum vessel on JT-60SA with high accuracy," *Fusion Eng. Des.*, vol. 125, pp. 1–8, Dec. 2017.

[6] A. Dans, P. Jucker, A. Bayon, J.-F. Arbogast, J. Caixas, J. Fernández, G. Micó, J. Pacheco, A. Trentea, and V. Stamos, "Challenging issues in the design and manufacturing of the European sectors of the ITER vacuum vessel," *Fusion Eng. Des.*, vol. 89, nos. 7–8, pp. 1769–1774, Oct. 2014.

[7] J. Ma, J. Wu, Z. Liu, H. Ji, and X. Fan, "NG-TIG welding technology research on 1/8 sector of CFETR vacuum vessel," *Fusion Eng. Des.*, vol. 152, Mar. 2020, Art. no. 111453.

[8] H. Wu, H. Handroos, P. Pela, and Y. Wang, "IWR-solution for the ITER vacuum vessel assembly," *Fusion Eng. Des.*, vol. 86, nos. 9–11, pp. 1834–1837, Oct. 2011.

[9] J. Eguia, L. Uriarte, A. Lamikiz, and A. Fernandez, "Main challenges in the development of a serial kinematic portable machine for the ITER vacuum vessel," *Fusion Eng. Des.*, vol. 92, pp. 16–28, Mar. 2015.

[10] H. Wu, Y. Wang, M. Li, M. Al-Saedi, and H. Handroos, "Chatter suppression methods of a robot machine for ITER vacuum vessel assembly and maintenance," *Fusion Eng. Des.*, vol. 89, nos. 9–10, pp. 2357–2362, Oct. 2014.

[11] J. Eguia, R. Enparantza, L. Uriarte, and A. Lamikiz, "Concept design of high precision portable machines for the *in-situ* manufacturing of the ITER vacuum vessel," *Proc. 16th Int. Conf. Eur. Soc. Precis. Eng. Nanotechnol. (EUSPEN)*, May 2016, pp. 2–3.

[12] K. Masaki, Y. K. Shibama, S. Sakurai, K. Shibanuma, and A. Sakasai, "JT-60SA vacuum vessel manufacturing and assembly," *Fusion Eng. Des.*, vol. 87, nos. 5–6, pp. 742–746, Aug. 2012.
[13] J. P. Merlet, "Jacobian, manipulability, condition number, and accuracy of parallel robots," *J. Mech. Des.*, vol. 128, no. 1, pp. 199–206, Jan. 2006.
[14] G. Liu, S. Zheng, X. Liu, Y. Wang, and J. Han, "Optimal design of the Gough–Stewart platform using evolutionary algorithms," *J. Harbin Inst. Technol.*, vol. 45, no. 3, pp. 39–44, Mar. 2013.
[15] S. V. Sreenivasan, K. J. Waldron, and P. Nanua, "Closed-form direct displacement analysis of a 6–6 Stewart platform," *Mech. Mach. Theory*, vol. 29, no. 6, pp. 855–864, Aug. 1994.
[16] F. Gao, W. Li, X. Zhao, Z. Jin, and H. Zhao, "New kinematic structures for 2-, 3-, 4-, and 5-DOF parallel manipulator designs," *Mech. Mach. Theory*, vol. 37, no. 11, pp. 1395–1411, Nov. 2002.
[17] Y. D. Patel and P. M. George, "Parallel manipulators applications—A survey," *Mod. Mech. Eng.*, vol. 2, no. 3, pp. 57–64, 2012.
[18] C. Gosselin, *Kinematic Analysis, Optimization and Programming of Parallel Robotic Manipulators*, vol. 252. Montreal, QC, Canada: McGill Univ., Aug. 1988.
[19] T. Yoshikawa, "Manipulability of robotic mechanisms," *Int. J. Robot. Res.*, vol. 4, no. 2, pp. 3–9.
[20] Z. Gao and D. Zhang, "Performance analysis, mapping, and multiobjective optimization of a hybrid robotic machine tool," *IEEE Trans. Ind. Electron.*, vol. 62, no. 1, pp. 423–433, Jan. 2015.
[21] Z. Gao, D. Zhang, X. Hu, and Y. Ge, "Design, analysis, and stiffness optimization of a three degree of freedom parallel manipulator," *Robotica*, vol. 28, no. 3, pp. 349–357, May 2010.
[22] D. Zhang and Z. Gao, "Forward kinematics, performance analysis, and multi-objective optimization of a bio-inspired parallel manipulator," *Robot. Comput.-Integr. Manuf.*, vol. 28, no. 4, pp. 484–492, Aug. 2012.
[23] D. Zhang and Z. Gao, "Performance analysis and optimization of a five-degrees-of-freedom compliant hybrid parallel micromanipulator," *Robot. Comput.-Integr. Manuf.*, vol. 34, pp. 20–29, Aug. 2015.
[24] Z. Chi, D. Zhang, L. Xia, and Z. Gao, "Multi-objective optimization of stiffness and workspace for a parallel kinematic machine," *Int. J. Mech. Mater. Des.*, vol. 9, no. 3, pp. 281–293, Sep. 2013.
[25] Z. Zhao, Z. Wu, J. Lu, W. Chen, and G. Zong, "Dynamic dexterity of redundant manipulators," in *Proc. IEEE Int. Conf. Syst., Man Cybern.*, vol. 1, Oct. 1995, pp. 928–933.
[26] G. Cui, D. Zhang, H. Zhou, and Y. Zhang, "Operating dexterity optimization and analysis of a 3-DOF parallel manipulator for a tunnel segment assembly system," *Int. J. Mech. Mater. Des.*, vol. 11, no. 3, pp. 277–285, Sep. 2015.
[27] F. A. Lara-Molina, D. Dumur, and K. A. Takano, "Multi-objective optimal design of flexible-joint parallel robot," *Eng. Comput.*, vol. 35, no. 8, pp. 2775–2801, 2018.
[28] J. Yao, W. Gu, Z. Feng, L. Chen, Y. Xu, and Y. Zhao, "Dynamic analysis and driving force optimization of a 5-DOF parallel manipulator with redundant actuation," *Robot. Comput.-Integr. Manuf.*, vol. 48, pp. 51–58, Dec. 2017.
[29] L. Xu, Q. Li, N. Zhang, and Q. Chen, "Mobility, kinematic analysis, and dimensional optimization of new three-degrees-of-freedom parallel manipulator with actuation redundancy," *J. Mech. Robot.*, vol. 9, no. 4, Aug. 2017.
[30] R. Ur-Rehman, S. Caro, D. Chablat, and P. Wenger, "Multi-objective path placement optimization of parallel kinematics machines based on energy consumption, shaking forces and maximum actuator torques: Application to the orthoglide," *Mech. Mach. Theory*, vol. 45, no. 8, pp. 1125–1141, Aug. 2010.
[31] X.-J. Liu, J. Wang, and G. Pritschow, "On the optimal kinematic design of the PRRRP 2-DoF parallel mechanism," *Mech. Mach. Theory*, vol. 41, no. 9, pp. 1111–1130, Sep. 2006.
[32] M. Russo, S. Herrero, O. Altuzarra, and M. Ceccarelli, "Kinematic analysis and multi-objective optimization of a 3-UPR parallel mechanism for a robotic leg," *Mech. Mach. Theory*, vol. 120, pp. 192–202, Feb. 2018.
[33] K. Deb, A. Pratap, S. Agarwal, and T. Meyarivan, "A fast and elitist multiobjective genetic algorithm: NSGA-II," *IEEE Trans. Evol. Comput.*, vol. 6, no. 2, pp. 182–197, Apr. 2002.
[34] J.-P. Merlet, "Jacoiban, manipulability, condition number, and accuracy of parallel robots," *ASME J. Mech. Des.*, vol. 128, no. 1, pp. 199–206, 2006.
[35] B. Ouyang and W. Shang, "Wrench-feasible workspace based optimization of the fixed and moving platforms for cable-driven parallel manipulators," *Robot. Comput.-Integr. Manuf.*, vol. 30, no. 6, pp. 629–635, Dec. 2014.
[36] C. Gosselin and J. Angeles, "A global performance index for the kinematic optimization of robotic manipulators," *J. Mech. Des., Trans. ASME*, vol. 113, no. 3, pp. 220–226, 1991.
[37] L.-W. Tsai and S. Joshi, "Kinematics and optimization of a spatial 3-UPU parallel manipulator," *J. Mech. Des., Trans. ASME*, vol. 122, no. 4, pp. 439–446, Dec. 2000.
[38] X.-J. Liu, J. Wang, and G. Pritschow, "Performance atlases and optimum design of planar 5R symmetrical parallel mechanisms," *Mech. Mach. Theory*, vol. 41, no. 2, pp. 119–144, Feb. 2006.
[39] G. Wu, S. Bai, and P. Hjørnet, "Architecture optimization of a parallel Schönflies-motion robot for pick-and-place applications in a predefined workspace," *Mech. Mach. Theory*, vol. 106, pp. 148–165, Dec. 2016.
[40] M. Li, H. Wu, and H. Handroos, "Static stiffness modeling of a novel hybrid redundant robot machine," *Fusion Eng. Des.*, vol. 86, nos. 9–11, pp. 1838–1842, Oct. 2011.
[41] K. Deb and H. Jain, "An evolutionary many-objective optimization algorithm using reference-point-based nondominated sorting approach. Part I: Solving problems with box constraints," *IEEE Trans. Evol. Comput.*, vol. 18, no. 4, pp. 577–601, Aug. 2014.
[42] Z. Xie, F. Xie, X.-J. Liu, J. Wang, and X. Shen, "Parameter optimization for the driving system of a 5 degrees-of-freedom parallel machining robot with planar kinematic chains," *J. Mech. Robot.*, vol. 11, no. 4, Aug. 2019, Art. no. 041003.
[43] Z. Chi, "Multi-objective optimization of stiffness and workspace for a parallel kinematic machine," in *Proc. ASME Int. Design Eng. Tech. Conf. Comput. Inf. Eng. Conf., 36th Mechanisms Robot. Conf., Parts A B*, vol. 4, Chicago, IL, USA, Aug. 2012, pp. 485–495.
[44] P. Xu, B. Li, C.-F. Cheung, and J.-F. Zhang, "Stiffness modeling and optimization of a 3-DOF parallel robot in a serial-parallel polishing machine," *Int. J. Precis. Eng. Manuf.*, vol. 18, no. 4, pp. 497–507, Apr. 2017.

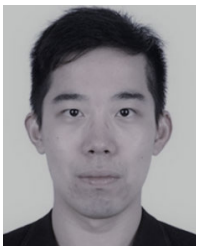

CHANGYANG LI was born in Jingzhou, Hubei, China, in 1994. He received the M.S. degree in mechanical engineering from the Lappeenranta University of Technology (LUT), Lappeenranta, Finland, in 2018, where he is currently pursuing the Ph.D. degree in mechanical engineering. Since 2018, he has been a Junior Researcher with LUT. His research interests include the design and development of robot systems for EU fusion reactors.

HUAPENG WU was born in China, in 1964. He received the D.Sc. (Tech.) degree from the Lappeenranta University of Technology (LUT), Lappeenranta, Finland, in 2001. Since 2004, he has been an Associate Professor with LUT, where he was a Professor, from 2008 to 2011. He has published four books and more than 100 publications in his areas of research. His research interests include robotics, AIT control, mechatronics, mechanical manufacturing, and automation.

HARRI ESKELINEN was born in Finland, in 1960. He received the M.S. and D.Sc. (Tech.) degrees from the Lappeenranta University of Technology (LUT), Lappeenranta, Finland, in 1987 and 1999, respectively. In 2000, he was nominated to be an Associate Professor in industrial engineering. In 2001, he was nominated to be an Adjunct Professor in DFMA. His main expertise covers the overlapping and integrated areas of product design, manufacturing and material selection. He is also the Head of the degree programs in mechanical engineering with LUT.